Impact of machining control variables on the surface roughness and kerf taper angle in the AWJC of A356 - 10 wt.% Al_2O_3 functionally graded composite

S. Prathap Singh*, *J.* Ajay, and *M.* Akash

Department of Mechanical Engineering, St Joseph's Institute of Technology, Chennai, Tamil Nadu, India

Abstract. This study delves into the topic of Abrasive Water Jet Cutting (AWJC) of Functionally Graded Composites (FGCs) made of Al6061-10 wt.% Alumina (Al_2O_3) through stir casting and horizontal centrifugal casting. Specifically, it examines how various cutting parameters affect surface roughness and kerf taper angle. Three separate zones were identified by microstructural analysis and Vickers microhardness testing in the manufactured FGC: an intermediate zone, a zone lacking in Al_2O_3, and an enriched zone. It is possible for the particle-dense area to reach a maximum hardness of 108 HV. Using a Taguchi L9 orthogonal array, machining trials were carried out on the Al_2O_t-rich zone, with feed, stand-off length, and abrasive supply rate being adjusted. By analyzing the Signal-to-Noise Ratio (SNR) and Analysis of Variance (ANOVA), it was shown that surface roughness was mainly affected by feed (47.11%), whereas kerf taper angle was mainly dictated by abrasive supply rate (78.12%). In order to minimize both responses, the optimal feed rate, stand-off length, and abrasive supply rates were found to be 10 mm/min, 1 mm, and 500 g/min, respectively. The creation of thicker chips, intensified particle collisions, and wider top kerfs was caused by increasing the feed and abrasive supply rates. As a result, surface roughness and kerf taper were enhanced. Machined surfaces analyzed with High-Resolution Scanning Electron Microscopy (HRSEM) showed plough marks, pits, ridges, and imbedded abrasives. These features became more pronounced as the abrasive supply rates were increased.

1 Introduction

Al composites serve application in technical fields such as aerospace and automotive due to its low density, wear resistance, and remarkable strength-to-weight ratio. Reinforcement particles made of ceramic materials, including oxides, carbides, and nitrides, can improve these qualities. The fast change in interfacial characteristics poses a threat to the success of traditional composites, notwithstanding their promise [1]. For these problems, Functionally Graded Composites (FGC) are the way to go. Unlike composites, FGMs are constantly

* Corresponding author: prathap.singh50@gmail.com

changing in composition and microstructure. The materials' improved responsiveness to deformation, dynamic loading, corrosion, and wear is a result of this progressive development, which in turn makes them applicable to a broad variety of industrial uses that demand varied properties [2].

Making parts with these top-notch specs and functionality is a fulfilling task. Components with enhanced properties are created by transport-aided centrifugal casting, which results in structures similar to a net. The target location was targeted for the delivery of secondary reinforcement particles using centrifugal force. To make the desired shape, molten metal is transferred to a spinning mold using a centrifugal casting process. The next step was to create a gradient sector in the middle and then split areas with reduced and enhanced features. Centrifugal force, particle size, melting temperature, cooling speed, density of molten liquid and reinforcing particles, and other parameters were used to define regions. It is possible to carry ceramic pieces with a lower density to the spin axis via a road. Denser elements, on the other hand, tend to shift away from the spin axis. Aerospace, military, automotive, power, electrical, and biomedical engineering are just a few of the fields that can benefit from these advanced materials [3].

The enhanced mechanical properties of FGCs strengthened with Silicon Nitride (Si_3N_4) and Silicon Carbide (SiC) are a result of the higher particle concentration and faster rotational speed achieved by centrifugally cast FGCs. Composites exhibit impressive increases in tensile strength and particle concentration throughout, but especially in their outer layers. Excessive reinforcing might cause specimen failure because of low bonding and high brittleness [4,5,6]. The outer layers of Al alloy strengthened with SiC showed the hardest features, according to research on Brinell hardness. This is because of the high attention of SiC elements. Comparative property tests revealed that the wear opposition of SiC/Al homogeneous MMCs was lower [7]. This result is owing to the statement that the SiC elements create strong intermetallic connections that resist deformation and contact forces. Waste drop, energy effectiveness, and environmental influence drop are the primary concerns of lean and green production, rather than productivity, surface quality, or dimensional correctness. New requirements have emerged, and producers may choose different techniques to meet them. This decision comes with benefits and drawbacks. An eco-friendly way to remove material is AWJC machining. Because it processes most materials without creating heat or harmful by-products, AWJC machining is environmentally benign. In a small-scale investigation of Al alloy machining, former investigators were present [8, 9].

The AA6026, reinforced with different weight percent SiC Metal Matrix Composites (MMC), was subjected to the AWJC by Gowthama et al. Reducing the SiC intensity increases surface roughness at portable speed and standoff height, according to the response. Critical variables such as traverse speed and stand-off distance influence the increase in volumetric removal rate and kerf angle with increased SiC loading [10]. An investigation of the Al7075 alloy strengthened with a hybrid of boron carbide and zirconium silicate was carried out by Thamizhvalavan et al. in an AWJC paper. As per a machining experiment, the rate of material removal is improved with slighter mesh magnitudes and greater ceramic supply proportions, but the kerf taper angle and surface roughness are decreased [11]. An AWJM examination was carried out by Prathap et al. on their Al 6061 alloy that was a hybrid nano MMC strengthened with SiC and boron carbide. The most important cutting variable, according to investigational material removal rate tests, is jet force (72.28%). The size of the abrasive particles accounts for 74.59% of the variation in surface roughness when cutting [12]. Researchers Hang et al. used the AWJC facility to drill a dump in Al2024-T3 Al base matrix alloy. The consequences show that at the given traverse speed, the ceramic mass stream rate affects outcomes, whereas liquid jet force has the greatest effect on perpendicularity and circularity, standoff height on kerf angle, and surface roughness [13].

Unlike typical MMCs, which frequently exhibit abrupt changes in characteristics at reinforcement-matrix interfaces, FGCs offer a smooth shift in composition and microstructure across their cross-section. This gradient distribution improves mechanical response in wear, impact, and dynamic loading conditions, making FGCs ideal for demanding engineering applications. While various studies have reported AWJC of homogeneous Al MMCs, little work has been done on machining functionally graded systems, where the existence of discrete ceramic-rich, intermediate, and depletion zones can dramatically affect machinability. This study examines the impression of important AWJC constraints on the exterior machined surface quality and kerf taper of Al6061-10 wt.% Al_2O_3 FGC, offering new insights for optimizing cutting performance in gradient materials.

2 Materials and methodology

2.1 Materials and manufacture

After the stir casting process, the Al 6061 base matrix strengthened 10 wt.% Al_2O_3 FG composite was made utilizing the economically beneficial horizontal centrifugal moulding. The graphite crucible was used to heat the Al6061 alloy pieces to 740°C in the electrical resistance furnace. The process of making FGC is illustrated in Figure 1(a) using an electrical resistance boiler. In order to avoid casting defects and reactions, the melting furnace was supplied with argon gas. In order to minimize temperature variations that could occur during the casting process, the Al_2O_3 reinforcing particles were heated to 250°C in a muffle boiler to remove any remaining moisture. Also, to make the reinforcement particles more wettable, a piece of magnesium (Mg) with a weight percentage of 1% was added. A hopper mounted atop the furnace allowed the gradual addition of preheated Al_2O_3 components to the molten Al metal.

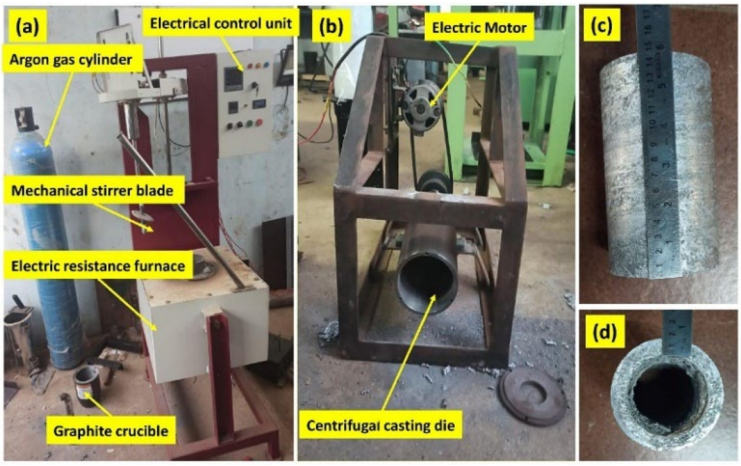

Fig. 1. (a) Stir moulding apparatus for creating molten form, (b) Horizontal centrifugal moulding apparatus for making hollow cylindrical component, (c) Top ,and (d) Front directional image of the manufactured FGC.

Particles of Al base matrix alloy and Al_2O_3 were thoroughly mixed by mechanical stirring at 500 rpm. The melt was transferred from the 850°C furnace to a 350°C horizontal centrifugal moulding die, which had an 85 mm innermost nominal diameter and a 140 mm distance and was set to rotate at 1200 rpm. Reducing solidification time and facilitating reinforcement mobility to the exterior periphery, preheating the centrifugal moulding die is

a worthwhile process. Figure 1(b) depicts the horizontal centrifugal casting facility. The rotating die was driven by the motor's circular motion using belts and pulleys. The molten metal was solidified while the rotating die rotated. The specimen with dimensions of 90 mm for outside diameter, 60 mm for inner diameter, and 150 mm for span is shown in Figure 1(c). It contains 10 weight percent Al_2O_3.

2.2 Mechanical and microstructural outcome

Using a 100 gf dead weight load and a 10-second settle duration from the outer to innermost boundary (1-15 mm), Vicker's microhardness experimentation adhered to ASTM-E384. The average of five measurements was used to determine the location's Vicker's microhardness. The dissemination of Al_2O_3 oxide strengthening elements along the casting's radial width was determined by studying the optical microstructure of the manufactured FGC with an Olympus upright metallurgical microscope. We started by collecting FGC samples (10 x 10 x 10 mm) from different places and cutting them using WEDM.

Using Al_2O_3 cloth and ceramic sheet papers ranging from 220 to 2000 grit, a number of FGC samples that had been wire-sliced were polished. To achieve the final polish, diamond paste with a particle size of 0.5 µm was utilized. Lastly, using Keller's surface morphology solution, the surface was etched. The BRUKER USA D8 Advance Davinci type, which ranges from 0.101 to 117.813, was utilized for the X-ray Diffraction (XRD) investigation. The minimum step size was 0.029.

2.3 Machining experiment

An Al_2O_3-rich area, situated 5 mm from the external borderline of the FG composite made of an Al 6061 base matrix strengthened with 10 wt. % Al_2O_3, was sampled for this study. The pin, which measures 5 x 5 mm and is 50 mm deep, was extracted for this purpose. As seen in Figure 2, the setup incorporates an AWJC device. A straight drive pump and a dynamic cutting head are part of the arrangement. The system is designed to support an extreme cutting load of 1200 kg/m² and has an in-line accuracy requirement of ±0.05 mm.

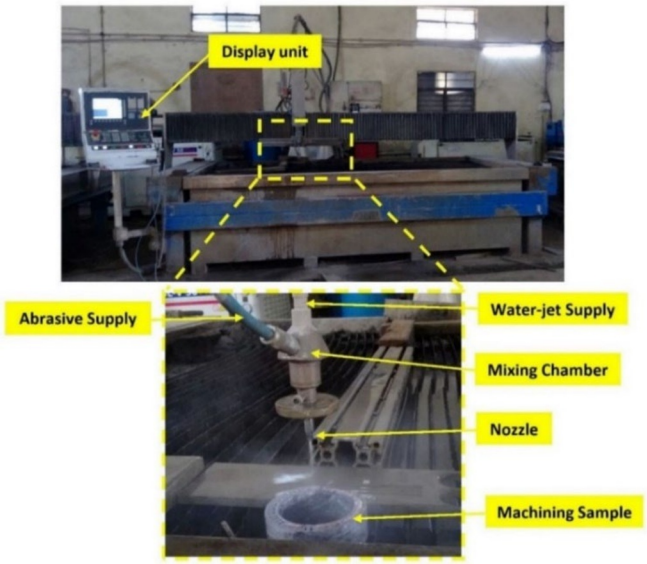

Fig. 2. AWJM arrangement utilized for the machining operation.

The cutting head has a mixing chamber that is designed to combine sand and water jets. The design incorporates a carbide nozzle with a 100-hour life expectancy and an aperture diameter of 0.1 mm. The material used is 80 mesh-size ceramic Al_2O_3 elements. With a supreme range of 200 mm, the cutting head may traverse along the Z-axis. Recorded traversal speeds reach 15,000 mm/min.

Using the Taguchi approach to implement Design of Experiments (DOE) is easy and intuitive. This method effectively reduces the breadth of study to a minimum required to draw valid conclusions. Feed, the distance among the jet nozzle and the machining FG composite sample (standoff height), and the rate of abrasive supply are the three input machining variables used in this experiment. Both the exterior surface quality and the kerf taper angle are used to describe the responses. Exterior surface roughness and kerf taper angle response were averaged from multiple measurements. A surface roughness tester (Make: Kosaka Laboratory Ltd, Japan; Model: SEF580AG18D) measured four surface roughness values on the machined surface and averaged them for each experiment. The kerf taper angle was calculated at three points of the cut piece using the video measuring system, and the mean was reported across trials. This method reduces the influence of randomness on measurement outcomes, enhancing the study's repeatability and statistical reliability.

To select the most suitable orthogonal array using Taguchi's methods, it is important to consider three key factors: This section lays out the key components, which include the input and response, along with the crucial relationships. There are two tiers of data for the machining control variables used as inputs. The experimentation yielded predictable consequences, including potential limitations in terms of efficiency and cost. The selection of the input machining variable ranges was based on current literature. Moreover, the prior investigations on AWJC and the input machining variables determined the feed (10–20 mm/min), standoff height (1 -2 mm), and abrasive supply rate (500 - 1500 g/min). These levels reflect lower and greater process extremes. Jet energy and particle velocity are sufficient for stable and precise cutting at lower feed and abrasive flow, while higher levels reveal surface deterioration due to excessive particle collisions and jet divergence.

The standoff height range was also chosen to explore jet focus and divergence on kerf geometry. Thus, the ranges specified ensure that the experimental design captures crucial AWJC machining control drilling variable effects on exterior surface quality and kerf taper angle while retaining process stability. Using Taguchi's L9 orthogonal array, the experimental strategy is supported. For the purpose of reproducibility, all machining trials were conducted using the same process conditions.

In MINITAB 17, the Taguchi approach is used to build the experimental design matrix. After doing the necessary research, a moveable surface roughness tester (Model: Surftest SJ-410, Make: Mitutoyo) is utilized to evaluate the surface roughness of the machined exterior. We average the results of five separate surface roughness evaluated values. Both the upper and lower channel widths are evaluated through the Video Measuring System (VMS). The kerf taper angle is determined by the measured reaction. As revealed in Figure 3, the kerf taper angle at the taper edge is determined by evaluating the inclination of the kerf wall. Plugging the workpiece's breadth into Equation (1) yields the kerf taper angle.

$$\theta = \tan^{-1}\left(\frac{W_t - W_d}{2t}\right) \quad (1)$$

The machined workpiece's thickness (t) and the top and bottom channel widths (W_t and W_d, respectively) are used here. Table 1 organizes the measured outcomes for extra scrutiny.

Table 1. Design plan and investigated outcomes.

Run No	Feed	Stand off height	Ceramic supply rate	Surface Roughness (μm)	Kerf taper angle (°)
1	10	1	500	2.93	1.77
2	10	1.5	1000	3.026	2.26
3	10	2	1500	3.799	2.61
4	15	1	1500	3.66	2.67
5	15	1.5	500	2.924	1.7
6	15	2	1000	3.774	2.41
7	20	1	1000	3.971	2.55
8	20	1.5	1500	4.901	3.2
9	20	2	500	3.736	2.15

3 Results and discussions

3.1 Outcome of Vicker's microhardness investigation

Vicker's microhardness scrutiny of the Al 6061 base matrix strengthened with 10 wt. % Al_2O_3 FGC is presented in Figure 3, measured at 2 mm intervals beside the centrifugal curve from the outer to the innermost periphery.

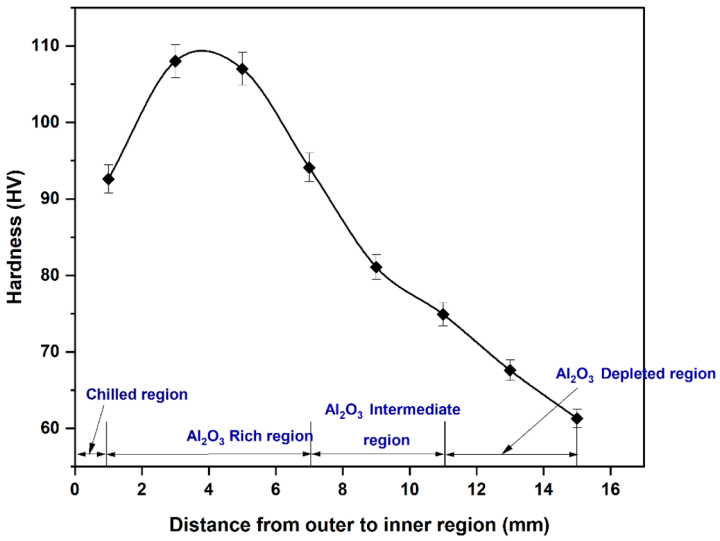

Fig. 3. Vicker's microhardness dissemination of the manufactured Al6061 FG composite.

Relative to the Al_2O_3-depleted area (11–15 mm), the Al_2O_3 zone with a higher particle concentration (1–7 mm) has a supreme Vickers microhardness of 109 HV, reflecting a 77%

enhancement. The improved wettability of the aluminum alloy and the distribution of Al_2O_3 ceramic reinforcing particles may be responsible. The density variation induced by centrifugal force leads to the primary Al_2O_3 reinforcement particles congregating at the outside perimeter of the FGC. Particle concentration and dispersion significantly enhance the hardness of the FGC. Amrit et al. detected comparable hardness in an Al-base matrix alloy strengthened with an element of 7.5 wt.% TiB_2 functionally categorized component [18]. A hardness gradient was detected in the Al_2O_3 intermediate location (7-11 mm), which was found between Al_2O_3-rich and Al_2O_3-depleted locations. Additionally, the microstructure of the FGC areas was scrutinized.

3.2 Microstructure scrutiny

Figure 4 illustrates the optical microscope microstructure outcome found from the optical microscope of the Al6061 base matrix alloy reinforced with 10 wt.% Al_2O_3 FG component. Figure 4(a) illustrates the peripheral boundary of the microstructure in the cooled region at a distance of 1 mm. The fast solidification of the molten mixture at the mold interface leads to a reduced concentration of reinforcement.

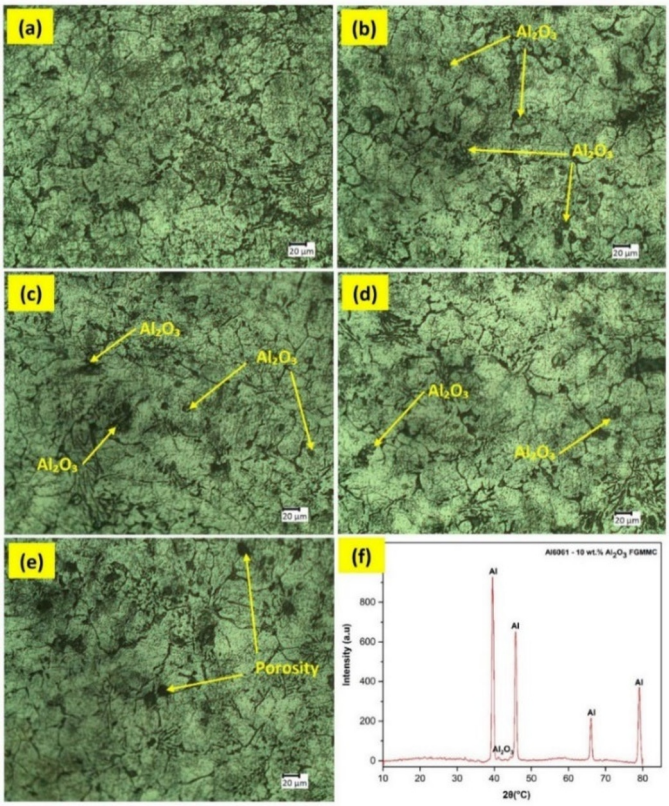

Fig. 4. Optical microstructure at dissimilar constituencies after the peripheral borderline of the FGC (a) Chill location (at 1 mm); (b) Al_2O_3 rich location (at 3 mm); (c) Al_2O_3 rich location (at 5 mm); (d) Al_2O_3 intermediate location (at 9 mm); (e) Al_2O_3 depleted location (at 13 mm), and (f) XRD.

Figures 4(b) and (c) illustrate the microstructure of the FG component specimen at 3 mm and 5 mm, respectively. In comparison to other microstructures, this one exhibits a superior dispersion of Al_2O_3 elements. Owing to Al's lower density compared to O_3, the high-density

particles are expelled to the outside boundary of the FGC by centrifugal force during the casting process. The Al_2O_3 particles are prevalent in this area. Saeh et al. identified a similarly elevated concentration of SiC strengthening in the area outside their Al matrix that was strengthened with 10 wt.% SiC FGC [19]. Figure 4(d) illustrates the FGC microstructure located 9 mm from the outside edge. This microstructure comprises a lower concentration of Al_2O_3 elements compared to the Al_2O_3-rich zone. This region serves as the intermediary for the Al_2O_3 element.

The microstructure of the FG component is illustrated in Figure 4(e) at a distance of thirteen millimeters from the outer edge. The microstructure of Al_2O_3 is diminished by centrifugal force. Region exhibiting a reduction in Al_2O_3 particles. We identified three separate zones: Al_2O_3 has element-rich, intermediate, and deficient compositions. Concentrated strengthening occurred in the element-rich zone, whereas the intensity of Al_2O_3 elements escalated from the Al_2O_3-exhausted to the Al_2O_3-intermediate locations. The dispersion of Al_2O_3 particles has a substantial effect on the characteristics of FGC. In both the Singh and Ananthapadmanaban aluminum alloys, there was a ceramic reinforcement gradient that was internally reinforced with silicon nitride FGC according to [11].

A quantitative assessment of reinforcement concentration was carried out on the optical micrographs captured at different radial locations using the image analysis program ImageJ to progress the comprehension of the gradient effect. The Al_2O_3-rich zone had an average reinforcement fraction of 20%, the Al_2O_3 intermediate zone had about 12%, and the Al_2O_3-depleted zone had less than 5% reinforcement. The gradual decrease in reinforcement fraction throughout the radial direction validates the functionally graded characteristics of the FGC.

An analysis using FGC XRD showed the attendance of Al alloy and strengthening elements in the Al 6061 alloy that had been increased with Al_2O_3 particles, as shown in Figure 4(f). According to JCPDS card no. 89-4037, base matrix of Al was discovered at elevations of 39.52°, 44.29°, 66.02°, and 79.04°. Also discovered at $2\theta = 41.12°$ (JCPDS card no. 46-121) were Al_2O_3 particles. The composite no longer showed any reaction by-products.

3.3 Examination of surface roughness

The Minitab application generated the SNR response table based on the SNRs of the associated surface roughness data. The cutting control variables, such as feed rate, standoff height, and abrasive supply rate, exert differing effects on exterior surface quality, as illustrated in Table 2. The impression of the machining governor variables was assessed using the delta value. The delta number was derived by subtracting the maximum and minimum SNR values from the machining variables. The feed rate significantly influenced surface roughness, continued by the ceramic supply proportion and standoff height.

Table 2. Mean SNR outcome for surface roughness.

Level	Feed	Standoff height	Ceramic supply rate
1	-10.18	-10.86	-10.04
2	-10.71	-10.91	-11.04
3	-12.41	-11.53	-12.22
Delta	2.23	0.66	2.19
Rank	1	3	2

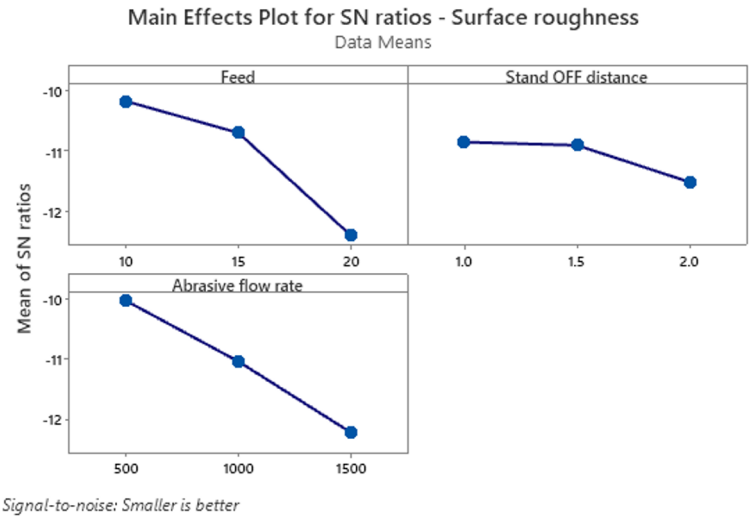

Fig. 5. Mean SNR chart for surface roughness.

Figure 5 displays the surface roughness and SNR graphs, and the optimal set of machining variables is determined by the maximum SNRs for each variable. A feed rate of 10 mm/min, a ceramic supply proportion of 500 g/min, and a standoff height of 1 mm were found to be the optimal set of machining factors for achieving lowest surface damages.

Table 3. Table of ANOVA consequences for the surface roughness.

Source	DF	Adj SS	Adj MS	F-Value	P-Value	Contribution (%)
Feed	2	2	1.50730	0.75365	5.89	47.91
Standoff height	2	2	0.09482	0.04741	0.37	3.01
Ceramic supply rate	2	2	1.28806	0.64403	5.03	40.94
Error	2	2	0.25593	0.12797		8.13
Total	8	8	3.14612			

The input-independent machining factors were tested for significance using ANOVA. The evaluation of ANOVA for surface quality and kerf taper angle was performed with a confidence interval of 95% and a significant level of 5%. Table 3 displayed the consequences of the analysis of variance (ANOVA) test for surface quality. After feed (47.91%) and abrasive supply rate (40.94%), standoff height (3.11%) and surface roughness were the most important factors for all three. Machining factors have a disproportionately large impact on feed surface roughness.

Figure 6 depicts the variation in surface roughness across several stages of each machining variable by presenting the data. The machining variable that most significantly affected surface roughness, as illustrated in the figure, indicated that an increase in feed resulted in heightened surface quality of the manufactured Al 6061 base matrix strengthened with 10 weight percent Al_2O_3 FG component. This benefit may be attributable to the development and elimination of denser chips when the feed speed is elevated. The thickness of the chips tends to exacerbate tool wear, perhaps adversely affecting exterior surface

superiority. Conversely, reduced feed rates usually yield enhanced surface performance properties by producing thinner chips and minimizing tool wear.

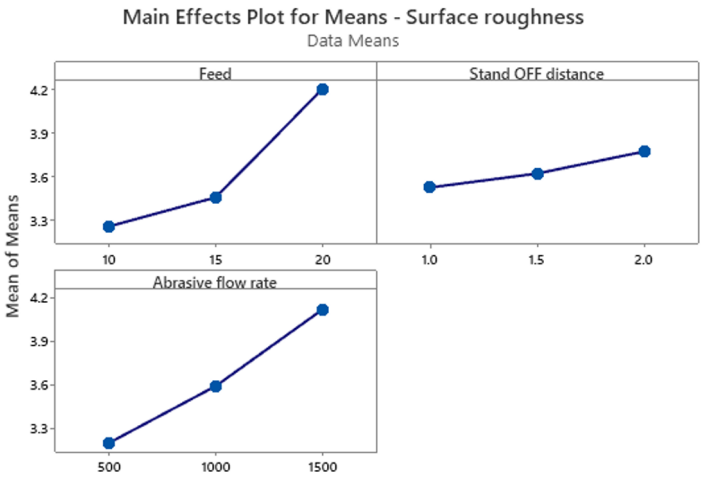

Fig. 6. Impact of cutting control variables on the surface roughness.

The surface quality of the FGC increased due to the elevated quantity of abrasive feed. Some faster abrasive feed rate outcomes in an increased number of abrasive elements contacting the surface, leading to a finish that is more uneven and harsh. Furthermore, particles may rebound from the workpiece surface and recontact it when the stand-off height is elevated. This exacerbates the existing surface flaws and roughness. Increased standoff heights yield less material removal efficiency, thereby producing a rougher surface. The kinetic energy of the ceramic particles diminishes as the standoff height increases.

3.4 Examination of kerf taper angle

Table 4 demonstrates the rank of the AWJ cutting control variables' effects on the kerf taper angle, including feed, standoff height, and ceramic supply proportion. The maximum effect of ceramic supply proportion on surface quality was observed, continued by feed and standoff height impressions.

Table 4. Mean SNR outcome for kerf taper angle.

Level	Feed	Standoff height	Ceramic supply rate
1	-6.791	-7.207	-5.406
2	-6.927	-7.265	-7.618
3	-8.294	-7.541	-8.989
Delta	1.503	0.334	3.583
Rank	2	3	1

Figure 7. displays the SNR and kerf taper angle graphs, and the optimal machining variables are those with the highest maximum SNRs. We found that 500 g/min of abrasive

supply, 10 mm/min of feed, and 1 mm of standoff height were the best machining parameters for accomplishing the slightest kerf taper angle.

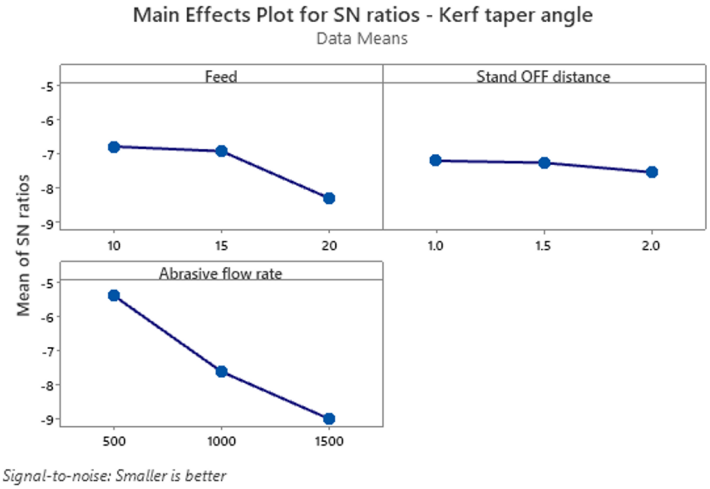

Fig. 7. Mean SNR graph for kerf taper angle.

Table 5. Table of ANOVA outcomes for the kerf taper angle.

Source	DF	Adj SS	Adj MS	F-Value	P-Value	Contribution (%)
Feed	2	0.31796	0.158978	7.00	0.125	18.27
Standoff height	2	0.00682	0.003411	0.15	0.869	0.39
Ceramic supply rate	2	1.36969	0.684844	30.15	0.032	78.72
Error	2	0.04542	0.022711			2.61
Total	8	1.73989				

Table 5 presents the results of the ANOVA employed to rank the machining variables. The abrasive supply rate (78.72%), feed (18.27%), and standoff height (0.39%) had the furthermost significant sound effects on surface roughness. The abrasive supply rate is a significant machining variable that induces the kerf taper angle.

Figure 8 depicts the dissimilarity in the kerf taper angle at distinct stages of the corresponding machining variable. The data designates that the kerf taper angle of the manufactured Al 6061 base matrix strengthened with 10 weight percent Al_2O_3 functionally disseminated component was enhanced with a growth in the ceramic supply proportion. This machining variable has the supreme impression on the kerf taper angle. A higher ceramic supply rate results in a greater number of abrasive elements contacting the material, which facilitates more effective FG component removal and a wider kerf at higher rates compared to lower rates.

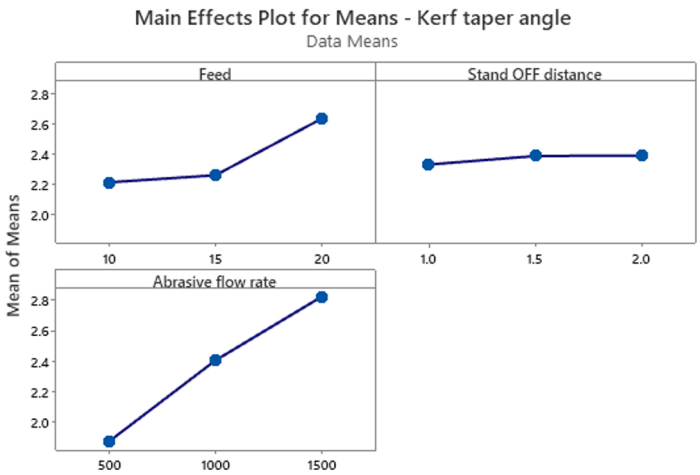

Fig. 8. Inspiration of machining control variables on the kerf taper angle.

The FGC's kerf taper angle also rose as a consequence of the feed rate increase. An even more dramatic change in channel width among the upper and bottommost of the cut caused by a greater feed rate makes the cut appear less vertical from the outside. The kerf taper angle will grow while the stand-off distance stays the same; as a result, A broader kerf at the apex and a greater taper angle are the results of a longer standoff height, which permits the ceramic components to separate further afore engaging the cutting material. This is the reasoning behind this scenario.

3.5 Machined surface evaluation

The exterior part was assessed utilizing HRSEM following AWJC to scrutinise the exterior features. Figure 9(a) presents the HRSEM appearance of the ceramic supply from the AWJ machined region, captured at a rate of 500 grams per minute. The machined surfaces exhibited reduced surface roughness, indicated by the presence of ridges, unfinished areas, ploughing symbols, and entrenched Al_2O_3 ceramic elements. The entrenched Al_2O_3 ceramic elements are generated because the ceramic elements lack sufficient energy. The elevation in surface roughness results from the minimal energy imparted to the ceramic elements when the ceramic solution's flow proportion is at its nadir.

Figure 9(b) presents the exterior surfaces of the HRSEM depiction of the AWJ drilled region at a ceramic supply rate of 1000 g/min. Cracks, completed exteriors, and entrenched Al_2O_3 ceramic elements on the machined exteriors were utilized to illustrate the material's surface roughness.

Figure 9(c) presents the visualized HRSEM image of the ceramic supply from the machined region, which was processed at a rate of 1500 grams per minute. The surface roughness was evidenced by deep depths, cutting wear, and entrenched Al_2O_3 ceramic elements on the drilled exteriors. Figure 9(d) depicts the drilled exterior EDS of the AWJ-machined exterior area. Only the components of the Al alloy and strengthening element were disclosed, and it was conclusively shown that the machining procedure did not produce any further reaction products.

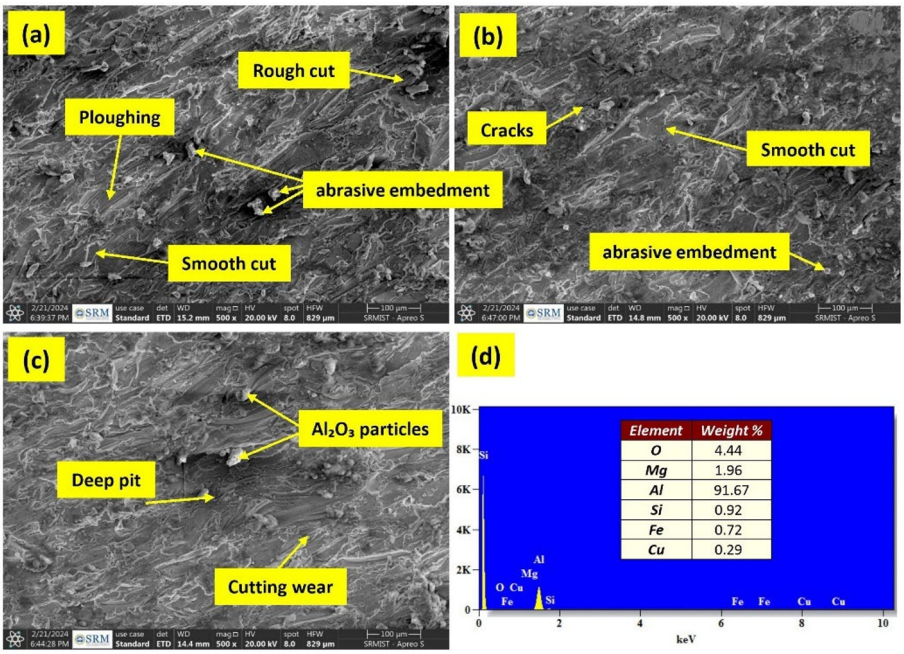

Fig. 9. HRSEM appearance of the machined exterior at dissimilar ceramic elements supply proportion (a) 500 g/min, (b) 1000 g/min, (c) 1500 g/min, and (d) Drilled exterior EDS of the AWJ machined exterior area.

4 Conclusion

A clear gradient in strengthening dissemination was observed in the Al 6061 - 10 weight percent Al_2O_3 FG component that was constructed through stir moulding and then subjected to horizontal centrifugal modeling. The outer zone, which was rich in particles, achieved a supreme Vickers microhardness of 109 HV, which is a 77% development over the region that was exhausted of particles.

The density-driven separation of Al_2O_3 under centrifugal pressure resulted in the formation of three separate zones, which were confirmed by optical microstructural analysis. These zones were classified as element-rich, intermediate, and element-depleted. As a result, the hardness and machinability of the material were directly influenced.

Using the Taguchi L9 orthogonal array experimental plan for AWJC, it was determined that feed was the most momentous cutting variable that had an effect on surface roughness (47.91%). Standoff height (3.11% of the total) and abrasive supply rate (40.94%) came next. A feed velocity of 10 mm/min, a ceramic supply proportion of 500 g/min, and a standoff height of 1 mm were the optimal conditions for attaining the lowest feasible surface roughness.

Ceramic element supply rate (78.72%), feed (18.27%), and standoff height (0.39%), in that order, were the cutting control variables that most affected the kerf taper angle. At a standoff height of one millimeter, a feed rate of ten millimeters per minute, and an abrasive supply rate of five hundred grams per minute were sufficient to accomplish the slightest kerf taper degree.

Output responses, such as surface roughness and kerf taper angle, increased with larger feed and abrasive supply rates. The primary causes of this were divergence and an increase

in abrasive impact energy. Conversely, increased standoff heights were associated with decreased cutting precision and particle scattering.

References

1. Runling Qian, Qiang Wang, Wenjuan Niu, Ning Hu.: The Influence of MoS_2 on Corrosion Behavior of B_4C-Reinforced Aluminium Composite Coatings by Cold Spray, JOM 77, 1671–1681, (2025).
2. Weiyi Liu, Zijin Zhang, Libiao Xin, Zhiqiang Li.: A multiscale finite element analysis model for functionally graded graphene reinforced composites considering graphene defects, Composite Structures, 371, 119499, (2025).
3. Prathap Singh S, Ananthapadmanaban D, Venkateshwaran N, Sai Balaji MA.: Effect of Ageing Temperature on the Hardness, Microstructural and Dry Sliding Wear Performance of the Functionally Graded A356 Alloy, International Journal of Metalcasting, 19, 955–976, (2025).
4. Vanam JP, Chiranjeevi R, Kumar RS, Ramana VV, Kumar AS.: Effect of SiC on Mechanical, Microstructure and Tribological properties of Aluminum MMC processed by Stir Casting, IOP Conf. Ser. Mater. Sci. Eng. 455, 012017 (2018).
5. Ambigai R, Prabhu S.: Analyzing the mechanical properties and characterization of aluminium (ADC-14) based functionally graded materials (FGM). Silicon 14, 2839-2850 (2022).
6. El-Galy IM, Ahmed MH, Bassiouny BI.: Characterization of functionally graded Al-SiCp metal matrix composites manufactured by centrifugal casting. Alex. Eng. J. 56, 371–381 (2017).
7. Surya MS, Prasanthi G.: Tribological behaviour of aluminum silicon carbide functionally graded material. Tribol. Ind. 40, 247–253 (2018).
8. Maurya M, Maurya NK, Bajpai V, Effect of SiC reinforced particle parameters in the development of aluminium based metal matrix composite. Evergreen 6, 200–206 (2019).
9. Lin Wu, Xiang Zou, Yuan Guo, Liandong Fu.: Experimental Research and Parameter Optimization of High-Pressure Abrasive Water Jet Machining, Lubricants, 13(4), 153, (2025).
10. Qasem, La'aly A. Al-Samrraie, Khalideh Al Bkoor Alrawashdeh.: Compressive Strength Impact on Cut Depth of Granite During Abrasive Water Jet Machining, Journal of manufacturing and materials processing, 9(8), 262, (2025).
11. Gowthama K, Somasheker HM, Suresha B, Bhagat Singh P, Rajini N, Faruq Mohammad, Hamad A Al-Lohedan, Ahmed A Soleiman.: Characterization and optimization of abrasive water jet machining parameters of aluminium/silicon carbide composites, Materials Research Express, 10, 115505, (2023).
12. Thamizhvalavan P, Varatharajulu M, Jagadeesh Baskaran.: Parametric optimization of abrasive waterjet machining for aluminum 7075/boron carbide/zirconium silicate hybrid composites, Proceedings of the Institution of Mechanical Engineers, Part E: Journal of Process Mechanical Engineering, 1-12, (2025).
13. Sundar Prathap Singh, Dhanigaivel Elil Raja, Dattaguru Ananthapadmanaban, Komparajan Vinoth Babu.: Exploring cutting parameters for enhanced performance in abrasive water jet machining of Al 6061 hybrid nanocomposite, Proceedings of the Institution of Mechanical Engineers, Part E: Journal of Process Mechanical Engineering, 1-15, (2025).